INTERNATIONAL JOURNAL FOR NUMERICAL AND ANALYTICAL METHODS IN GEOMECHANICS, VOL. 20, 79–99 (1996)

FINITE ELEMENT MODELLING FOR LAND DISPLACEMENTS DUE TO PUMPING

HUND-DER YEH

Institute of Environmental Engineering, National Chiao-Tung University, 75 Po-Ai St., Hsinchu, Taiwan 30039, R.O.C.

RUEY-HSING LU

Department of Civil Engineering, National Chiao-Tung University, Taiwan

AND

GOUR-TSYH YEH

Department of Civil and Environmental Engineering, Pennsylvania State University, University Park, PA 16802, U.S.A.

SUMMARY

Equations of equilibrium (force balance) and flow in multidimensions were coupled in this paper to describe land displacements due to pressure decline in aquifers. A Galerkin finite element model based on these equations was developed. The saturated/unsaturated behaviour and the isotropic/anisotropic properties of permeability and elasticity were considered when the model was formulated. This model was verified by comparing its simulation results with those of known analytical solutions for simplified cases. The simulation of displacements due to pressure decline in unsaturated media was also performed. Those results demonstrated that the choice of boundary ranges for an aquifer with infinite domain may significantly affect the estimated horizontal and vertical displacements. To obtain a good estimation of land displacements, the boundary ranges should be carefully chosen. The displacements occurring in unconfined aquifers are caused by the drop of the water table and the change in body force in the dewatering zone. Simulation results also indicated that the change in body force should be considered once an unconfined aquifer has been pumped. Otherwise, the horizontal and vertical displacements in unconfined aquifers would be overestimated and underestimated, respectively. The behaviour of land displacements due to pumping was shown to be affected by changes in the total stresses in aquifers.

KEY WORDS: Land displacement; groundwater pumping; Galerkin finite element model

INTRODUCTION

Heavy groundwater pumping has induced serious land displacement problems in several cities around the world. Pressure decline in confined and unconfined aquifers is accompanied by a change in effective stress in the solid skeleton. This change in effective stress then leads to land displacements. Most existing models merely predict the vertical displacement (i.e. subsidence). This assumption of one-dimensional subsidence allows for the elimination of a set of dependent variables and uncoupled equations can be derived. Uncoupling, however, occurs only under rather special circumstances and may lead to substantial errors. Horizontal displacement may be of the same order of magnitude as vertical displacement in some situations.[1] Real subsidence problems are coupled in nature in most situations and should be solved as such.[2] A physical system coupling four partial differential equations was first presented by Biot[3] to describe the phenomena of transient flow and displacements occurring in three-dimensional deforming porous media. On the basis of Biot's work, Bear and Corapcioglu[4, 5] proposed a mathematical

CCC 0363–9061/96/020079–21

Received 23 March 1993
Revised 29 June 1995

formulation for regional land displacement problems due to pumping from confined or unconfined aquifers. The finite element method has been widely used to simulate similar field problems. Safai and Pinder[6,7] constructed a Galerkin finite element model to simulate the land displacements and axisymmetric flow resulting from pumping in confined and desaturating systems. Gambolati and Freeze[8] and Gambolati *et al.*[9] simulated the subsidence of Venice using the finite element technique. Schrefler and Zhan[10] developed a fully coupled finite element model to simulate the slow transient phenomena of consolidation in porous media with variable saturation. Lloret *et al.*[11] also analysed the problems of flow and deformation based on consideration of some features of the behaviours of unsaturated soils. Lewis and Schrefler[12] employed the finite element method to simulate land displacement problems in the areas of soil mechanics and reservoir engineering.

The objective of this paper is to develop a general Galerkin finite element model and to study the behaviour of multidimensional land displacements due to pressure decline in aquifers. The saturated/unsaturated behaviour and the isotropic/anisotropic properties of permeability and elasticity are considered in the formulation of the developed model. The change in body force in unconfined aquifers, which is usually neglected in engineering practice, is also taken into consideration. The verification of this model is done in cylindrical co-ordinates by comparing simulation results obtained from it with known analytical solutions for simplified cases. Displacements in unsaturated media are then simulated. The influences of boundary and the change in body force on the simulations are demonstrated and discussed. The effect of changes in stresses on the displacement behaviour is also illustrated.

GOVERNING EQUATIONS

A general mathematical model describing land displacements due to pressure decline in aquifers may be formulated by coupling the transient flow equation and the equilibrium equation. The flow equation, which governs the distribution of the pressure head in deforming porous media, may be derived on the basis of (1) the continuity of fluid, (2) the continuity of solid, (3) the motion of fluid (Darcy's law), (4) the deformation/displacement of media and (5) the compressibility of fluid. Consequently, the flow equation for deforming porous media in Cartesian co-ordinates may be written as[13]

$$\nabla \cdot \mathbf{q}_r + S_w \frac{\partial}{\partial t}\left(\frac{\partial u_k}{\partial x_k}\right) + n\frac{\partial S_w}{\partial t} + n\beta_w S_w \frac{\partial P}{\partial t} = q, \quad k = x, y, z \tag{1}$$

where $\mathbf{q}_r = -\mathbf{K}\nabla\phi$ is Darcy's velocity, S_w is the degree of saturation, $\partial u_k/\partial x_k$ is the dilation of unit volume, u_k is the component of the displacement in the k direction, n is the porosity of media, β_w is the compressibility of the fluid, P is the pressure, q is the sink term, $\mathbf{K} = \mathbf{K}(S_w)$ is the hydraulic conductivity tensor which is a non-linear function in terms of the degree of saturation when the soil is in an unsaturated condition, $\phi = P/\rho g + z$ is the hydraulic head, ρ is the density of water, g is the gravitational acceleration and z is the elevation above the datum. The air pressure is commonly assumed to be atmospheric and may be neglected if the air and water phases are included in the unsaturated soil. The non-linear relationship between the degree of saturation S_w and the pressure P may be found by the retention curve in unsaturated media. Accordingly,

$$\frac{\partial S_w}{\partial t} = \frac{\mathrm{d}S_w}{\mathrm{d}P}\frac{\partial P}{\partial t}$$

may be obtained.

In the absence of inertial effects, the equilibrium of forces acting on porous media in Cartesian co-ordinates may be expressed as[14]

$$\frac{\partial \sigma_{ij}}{\partial x_j} + f_i = 0, \quad i, j = x, y, z \tag{2}$$

where σ_{ij} is the total stress tensor, $f_i = [\rho n S_w + (1 - n)\rho_s] g_i$ is the component of the body force in the i direction, ρ_s is the density of solid and g_i is the component of gravitational acceleration in the i direction. The relationship between stresses and pressure in Cartesian co-ordinates may be expressed as[13]

$$\sigma_{ij} = \sigma'_{ij} - S_w P \delta_{ij}, \quad i, j = x, y, z \tag{3}$$

where σ'_{ij} is the effective stress tensor and δ_{ij} is the Kronecker delta symbol. Equation (2) may be divided into two parts: the initial steady state, which is a state of equilibrium, and the incremental state. These two states may be expressed as[14]

$$\frac{\partial \sigma^0_{ij}}{\partial x_j} + f_i^0 = 0, \quad i, j = x, y, z \tag{4a}$$

and

$$\frac{\partial \sigma^e_{ij}}{\partial x_j} + f_i^e = 0, \quad i, j = x, y, z \tag{4b}$$

where the superscripts $(\cdot)^0$ and $(\cdot)^e$ denote the initial and incremental values of physical quantities, respectively. The initial steady state of equilibrium, equation (4a), may be omitted here.

According to the concepts introduced by Terzaghi,[15] the displacement of media may take place as a result of changes in the effective stresses. Media are assumed here to be elastic and cross-anisotropic (or transversely isotropic). Thus, the elastic-constitutive relationship for the media in Cartesian co-ordinates may be expressed by Hooke's law as

$$\begin{Bmatrix} \sigma'^e_{xx} \\ \sigma'^e_{yy} \\ \sigma'^e_{zz} \\ \sigma'^e_{xy} \\ \sigma'^e_{yz} \\ \sigma'^e_{zx} \end{Bmatrix} = \begin{bmatrix} 2N + A & A & F & 0 & 0 & 0 \\ A & 2N + A & F & 0 & 0 & 0 \\ F & F & C & 0 & 0 & 0 \\ 0 & 0 & 0 & N & 0 & 0 \\ 0 & 0 & 0 & 0 & L & 0 \\ 0 & 0 & 0 & 0 & 0 & L \end{bmatrix} \begin{Bmatrix} \varepsilon_{xx} \\ \varepsilon_{yy} \\ \varepsilon_{zz} \\ \varepsilon_{xy} \\ \varepsilon_{yz} \\ \varepsilon_{zx} \end{Bmatrix} \tag{5}$$

where A, C, F, L, and N are the material constants of cross-anisotropic media defined by Love[16] and $\varepsilon_{ij} = \frac{1}{2}(\partial u_i/\partial x_j + \partial u_j/\partial x_i)$ with $i, j = x, y, z$ is the component of the strain. $A = F = \lambda$, $L = N = G$ and $C = \lambda + 2G$ if the media are isotropic, where λ and G are known as Lame's constants. Supplemented by equation (5), equations (1) and (4b) constitute four non-linear partial differential equations with four dependent variables, P, u_x, u_y, and u_z.

FINITE ELEMENT APPROXIMATIONS

Equations (1), (4b) and (5) constitute a general mathematical statement of the physical problem of land displacements due to pressure decline in confined or unconfined aquifers. Analytical solutions for this general system are not available. Therefore, numerical approaches may be employed to solve the problem. A finite element approximation is chosen owing to its ability to treat compound regions and complex geometries.

Applying the Galerkin approach and Green's theorem to equations (1) and (4b) yields

$$\sum_{\alpha=1}^{N_{\text{node}}}\left[\int\left[-\nabla N_\alpha\cdot\mathbf{q}_r+N_\alpha S_w\frac{\partial}{\partial t}\left(\frac{\partial u_k}{\partial x_k}\right)+N_\alpha\left(n\frac{dS_w}{dP}+n\beta_w S_w\right)\frac{\partial P}{\partial t}\right]d\Omega\right.$$
$$\left.=-\int N_\alpha\mathbf{q}_r\cdot\mathbf{n}\,d\Gamma+\int N_\alpha q\,d\Omega\right],\quad k=x,y,z \tag{6}$$

and

$$\sum_{\alpha=1}^{N_{\text{node}}}\left[\int\frac{\partial N_\alpha}{\partial x_j}[\sigma'_{ij}-S_w P\delta_{ij}]^e\,d\Omega=\int N_\alpha f_i^e\,d\Omega+\int N_\alpha\sigma_{ij}^e n_j\,d\Gamma\right],\quad i,j=x,y,z \tag{7}$$

where N_α is the basis function, N_{node} is the total number of nodes in the region of interest Ω and n_j is the component of the outward unit vector n normal to the boundary Γ in the j direction. Let the trial solution of the dependent variable φ, which represents P, u_x, u_y, and u_z, be expressed in the form

$$\varphi\approx\hat{\varphi}=\sum_{\beta=1}^{N_{\text{node}}}\varphi_\beta(t)N_\beta(x,y,z) \tag{8}$$

where φ_β is the value of φ at node β. The effective stress in equation (7) may be expressed in terms of the displacement by utilizing the elastic-constitutive relationship, i.e. equation (5). The trial solution, equation (8), may then be employed to rewrite equations (6) and (7) in a matrix form as

$$\begin{aligned}
&[C_{11}]\left\{\frac{dP}{dt}\right\}+[C_{12}]\left\{\frac{du_x}{dt}\right\}+[C_{13}]\left\{\frac{du_y}{dt}\right\}+[C_{14}]\left\{\frac{du_z}{dt}\right\}+[C_{15}]\{P\}=\{R_1\}\\
&[C_{21}]\{P^e\}+[C_{22}]\{u_x\}+[C_{23}]\{u_y\}+[C_{24}]\{u_z\}=\{R_2\}\\
&[C_{31}]\{P^e\}+[C_{32}]\{u_x\}+[C_{33}]\{u_y\}+[C_{34}]\{u_z\}=\{R_3\}\\
&[C_{41}]\{P^e\}+[C_{42}]\{u_x\}+[C_{43}]\{u_y\}+[C_{44}]\{u_z\}=\{R_4\}
\end{aligned} \tag{9}$$

where $\{\cdot\}$ is a column vector whose components are the values of dependent variables at nodes or a load vector on the right-hand side; $d(\cdot)/dt$ is the derivative of the dependent variable with respect to time and $[\cdot]$ is the coefficient matrix. The definitions of coefficient matrix and load vectors in Cartesian co-ordinates and in cylindrical co-ordinates are listed in Appendix I.

Employing the formula of finite differences, time derivatives in equation (9) may be written as

$$\left\{\frac{d\varphi}{dt}\right\}=\frac{\{\varphi\}_t-\{\varphi\}_{t-\Delta t}}{\Delta t},\quad \varphi=P,u_x,u_y,u_z \tag{10}$$

in which $\{\varphi\}_t$ and $\{\varphi\}_{t-\Delta t}$ are the values of $\{\varphi\}$ evaluated at time t and $t-\Delta t$, respectively, and Δt is the step-size of time. The vector of variable increment $\{P^e\}$ in equation (9) may be expressed as $\{P^e\}=\{P\}_t-\{P\}_{t=0}$ where $\{P\}_{t=0}$ is the value of pressure prescribed at the initial time. With the assistance of equation (10), the final matrix system may be written as

$$\begin{aligned}
&[C_{PP}]\{P\}+[C_{Pu_x}]\{u_x\}+[C_{Pu_y}]\{u_y\}+[C_{Pu_z}]\{u_z\}=\{R_P\}\\
&[C_{u_xP}]\{P\}+[C_{u_xu_x}]\{u_x\}+[C_{u_xu_y}]\{u_y\}+[C_{u_xu_z}]\{u_z\}=\{R_{u_x}\}\\
&[C_{u_yP}]\{P\}+[C_{u_yu_x}]\{u_x\}+[C_{u_yu_y}]\{u_y\}+[C_{u_yu_z}]\{u_z\}=\{R_{u_y}\}\\
&[C_{u_zP}]\{P\}+[C_{u_zu_x}]\{u_x\}+[C_{u_zu_y}]\{u_y\}+[C_{u_zu_z}]\{u_z\}=\{R_{u_z}\}
\end{aligned} \tag{11}$$

in which the definitions of the coefficient matrices and the load vectors in equation (11) are listed in Appendix II.

MODEL VERIFICATION

To verify the finite element model, three simplified cases with known solutions are utilized. Cylindrical co-ordinates are employed for all of the following cases.

A regional case for a single well pumping from a confined aquifer

A single fully penetrating well of radius r_w pumping at a constant rate Q_w from a confined aquifer with horizontal infinite extent is considered. The formation of this aquifer is homogeneous and isotropic. The initial thickness of the aquifer system is assumed to be uniform in space. The initial and boundary conditions for such an aquifer system with $i, j = r, z$ are described as

$$\begin{aligned}
&t \leqslant 0, \quad r \geqslant r_w, && \phi = \phi^0 \quad \text{and} \quad u_r,\ u_z = 0 \\
&t > 0, \quad r = r_w, && \frac{\partial \phi}{\partial r} = \frac{Q_w}{2\pi r_w K B} \quad \text{and} \quad u_r = 0,\ \sigma^e_{zj} n_j = 0 \\
&t > 0, \quad r \to \infty, && \phi = \phi^0 \quad \text{and} \quad \sigma^e_{ij} n_j = 0 \\
&t > 0, \quad z = B, && \frac{\partial \phi}{\partial z} = 0 \quad \text{and} \quad e^e_{ij} n_j = 0 \\
&t > 0, \quad z = 0, && \frac{\partial \phi}{\partial z} = 0 \quad \text{and} \quad u_z = 0,\ \sigma^e_{rj} n_j = 0
\end{aligned} \tag{12}$$

where u_r is the horizontal displacement in cylindrical co-ordinates, B is the saturated thickness of the aquifer, and $\mathbf{K} = K$ is a constant for a homogeneous and isotropic aquifer. The magnitude of the vertical displacement is assumed here to be rather small as compared with the thickness of the compressible layer D. Consequently, B and D may be considered to be equivalent and constant in time, i.e. $D = B \simeq B^0$. Based on these assumptions, Bear and Corapcioglu[4] presented analytical solutions for the regional variables. These regional variables are the drawdown $s = \phi^0 - \phi$, the averaged horizontal displacement $\bar{u}_r$, which does not vary along the vertical direction of an aquifer, and the vertical displacement at the surface of the aquifer $u_z(r, z = B) = -\Delta z$.

The data from the paper of the Bear and Corapcioglu[4] are utilized for simulations: the transmissivity $T = KB = 95\ \text{cm}^2/\text{s}$; $B = D = 142$ m; $Q_w = 50$ l/s; $\gamma_w = \rho g = 9{\cdot}806 \times 10^{-3}\ \text{N/cm}^3$; and $\lambda = G = 4{\cdot}475 \times 10^3\ \text{N/cm}^2$. The water compressibility β_w is neglected. The non-uniform finite element mesh sketched in Figure 1 is employed to simulate the problem. The aquifer thickness is divided uniformly by the vertical grid-size $\Delta v = 28{\cdot}4$ m. In the horizontal direction, the horizontal grid-size Δr is non-uniform. The sizes of Δr are small near the well and gradually increase toward the infinite boundary. At $r = r_w = 0{\cdot}3$ m, a constant flux is specified and the soil is restrained from any lateral movement; however, it is free to move vertically. Both the top surface and bottom of the aquifer are treated as impervious, i.e. no flux across the impervious boundaries. At the top surface of the aquifer, i.e. the top boundary, the soil is free to move both vertically and horizontally. At the bottom of the aquifer, i.e. the bottom boundary, the soil is restrained from any vertical movement; however, it is free to move horizontally. A finite boundary $r = R$, chosen to be at a distance far from the well, is used in the numerical simulation to approximate the infinitely horizontal domain. The soil is treated as free to move both vertically and horizontally at $r = R$ (i.e. $\sigma^e_{ij} n_j = 0$ at $r = R$) in the numerical simulations, although the soil movement at $r \to \infty$ may be very small.

Results of simulations for the drawdown and displacements are shown in Figure 2. In the figures, the vertical displacement at the top surface Δz, the average of the drawdown s at the nodes

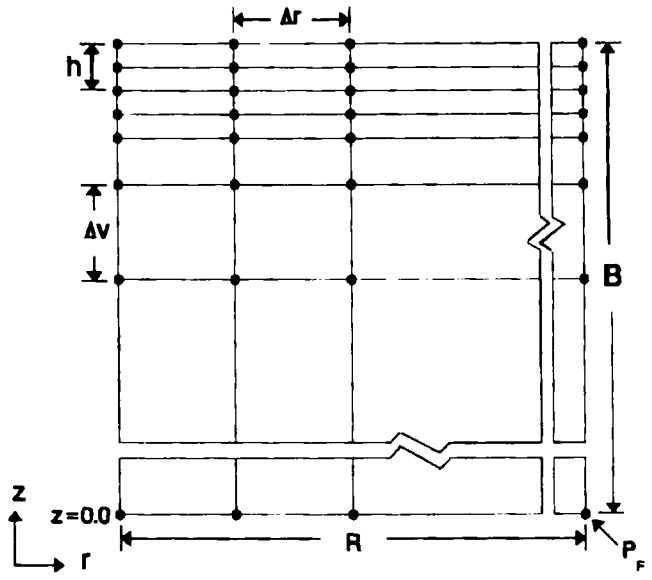

Figure 1. A finite element mesh in cylindrical co-ordinates

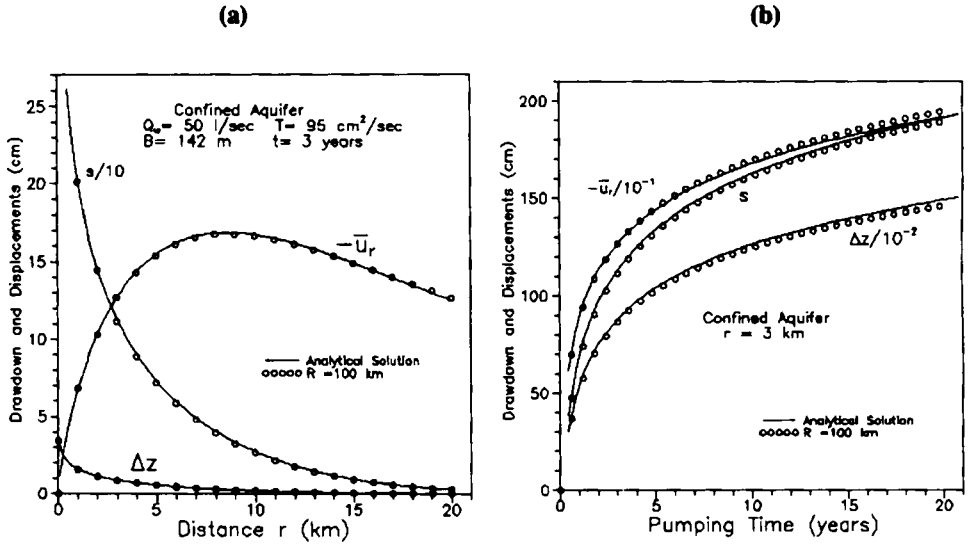

Figure 2. Distribution of the drawdown s, horizontal displacement $\bar{u}_r$ and vertical displacement Δz when pumping from a confined aquifer: (a) spatial distribution after continuous pumping for 3 yr and (b) temporal distribution at 3 km from the pumping well

along the vertical direction, and the average of the horizontal displacement $\bar{u}_r$ at the nodes along the vertical direction are taken to represent the regional variables. Simulations of chosen horizontal boundary range $R = 10$ km are demonstrated by circles. Analytical solutions[4] for the drawdown, horizontal displacement and vertical displacement are indicated by solid lines. The

relationship of the drawdown, horizontal displacement and vertical displacement versus the distance from the well after continuous pumping for 3 yr is shown in Figure 2(a). The relationship of the drawdown, horizontal dispalcement and vertical displacement versus time at a distance of 3 km from the well is shown in Figure 2(b). When the infinitely horizontal domain is considered, the horizontal displacements after continuous pumping for 3 yr are $-16{\cdot}781$ and $-12{\cdot}553$ cm, respectively, at distances of 10 and 20 km from the well. The minus values of displacements represent soil movement toward the pumping well, i.e. the centre of the horizontal co-ordinate. For the horizontal boundary range $R = 100$ km, the absolute errors[17] in estimated horizontal displacements are $-0{\cdot}144$ and $0{\cdot}044$ cm, respectively, at distances of 10 and 20 km from the well, as indicated in Figure 2(a). After continuous pumping for 20 yr, the drawdown, horizontal displacement, and vertical displacement at a distance of 3 km from the well are $191{\cdot}49$, $-19{\cdot}167$ and $-1{\cdot}490$ cm, respectively, when the infinitely horizontal domain is considered. The absolute errors in these estimated values are $1{\cdot}507$, $0{\cdot}209$ and $-0{\cdot}021$ cm, respectively, when $R = 100$ cm.

It is found from the simulation results that the estimated drawdown and displacements will be affected when the values of the horizontal boundary range R are less than 100 km. However, when the chosen horizontal boundary ranges are greater than 100 km, the simulation results do not change with increasing horizontal boundary ranges. Thus, simulation results with R greater than 100 km represent the solution for infinity domain and are compared with the analytical solutions for infinity domain. Results also demonstrate that the simulated drawdown and displacements match well with those of the analytical solutions when R is larger than 100 km. It indicates that caution should be taken when choosing the value of R for simulating the infinite domain problem.

A regional case for a single well pumping from an unconfined aquifer

A single fully penetrating well of radius r_w pumping at a constant rate Q_w from an unconfined aquifer with horizontal infinite extent is considered. The formation of this aquifer is homogeneous and isotropic. The initial thickness of the aquifer system is assumed to be uniform in space. The initial and boundary conditions for such an aquifer system with $i, j = r, z$ are described as

$$
\begin{aligned}
&t \leqslant 0, \quad r \geqslant r_w, \quad \phi = \phi^0 \quad \text{and} \quad s, u_r, u_z = 0 \\
&t > 0, \quad r = r_w, \quad \frac{\partial \phi}{\partial r} = -\frac{\partial s}{\partial r} = \frac{Q_w}{2\pi r_w K B} \quad \text{and} \quad u_r = 0, \sigma^e_{zj} n_j = 0 \\
&t > 0, \quad r \to \infty, \quad \phi = \phi^0 \quad \text{and} \quad \sigma^e_{ij} \cdot n_j = 0 \\
&t > 0, \quad z = \phi|_{F_h}, q_{r|F_h} \cdot \nabla F_h = S_y \frac{\partial \phi}{\partial t} = -S_y \frac{\partial s}{\partial t}, \sigma^e_{ij} n_j = 0 \\
&t > 0, \quad z = 0, \quad \frac{\partial \phi}{\partial z} = 0 \text{ and } u_z = 0, \sigma^e_{rj} n_j = 0
\end{aligned}
\tag{13}
$$

in which $F_h = z - \phi(r, t) = 0$ represents the phreatic surface (or water table) where the elevation head is equal to the hydraulic head $\phi(r, t)$ and S_y is the specific yield defined as the volume of pore water releated by unit decline in water table per unit area. The term $\mathbf{q}_r|_{F_h} \cdot \nabla F_h$ represents the flux across the phreatic surface and the term $S_y \partial\phi/\partial t$ represents the water released rate from the unconfined aquifer in response to the drop of the hydraulic head ϕ.

The magnitude of the drawdown s is assumed here to be rather small as compared with the saturated thickness B of the aquifer at any time. The magnitude of the vertical displacement at the surface of the aquifer is also assumed to be rather small compared with the thickness D of the

compressible layer. Also, B and D may be considered to be equivalent and constant in time. Based on the above assumptions, Lu and Yeh[18] presented the analytical solutions for the drawdown, averaged horizontal displacement and vertical displacement at the surface of the aquifers.

The data from the paper of Corapcioglu and Bear[5] are again utilized for simulations: $K = 6{\cdot}69 \times 10^{-3}$ cm/s; $B = D = 142$ m; $Q_w = 50$ l/s; $S_y = 0{\cdot}4$; $\gamma_w = \rho g = 9{\cdot}806 \times 10^{-3}$ N/cm^3; and $\lambda = G = 4{\cdot}475 \times 10^3$ N/cm^2. The water compressibility β_w is neglected. The non-uniform finite element mesh, which is the same as that used in the case of the confined aquifer, is employed again here. The effect of delayed yield in unconfined aquifers, i.e. the unsaturated effect, is neglected here, since it is insignificant for regional problems. The settings of aquifer boundaries are chosen to be the same as in the case of the confined aquifer except that the top surface is previous. Hence, the water table may drop as a consequence of pumping. The body force within the zone where the water table drops may change. This change may be considered to occur near the top boundary, since the drawdown is assumed to be rather small compared with the saturated thickness. The change in body force is equivalent to the weight of pore water in the dewatering zone.

Results of simulations are shown in Figure 3. Simulations of chosen horizontal boundary range $R = 60$ km, that larger chosen values would not change the estimated results, are demonstrated by circles. Results of simulations when the change in body force is neglected are also shown by dotted symbols. Analytical solutions,[18] which include the change in body force, for the drawdown, horizontal displacement and vertical displacement are indicated by solid lines. When the infinitely horizontal domain and the change in body force are considered, the horizontal displacements after continuous pumping for 3 yr are $-0{\cdot}789$ and $-0{\cdot}394$ cm, respectively, at distances of 10 and 20 km from the well, as shown in Figure 3(a). The absolute errors in estimated horizontal displacements at distances of 10 and 20 km from the well are 0·015 and 0·027 cm, respectively, when $R = 60$ km and including the change in body force. When neglecting the

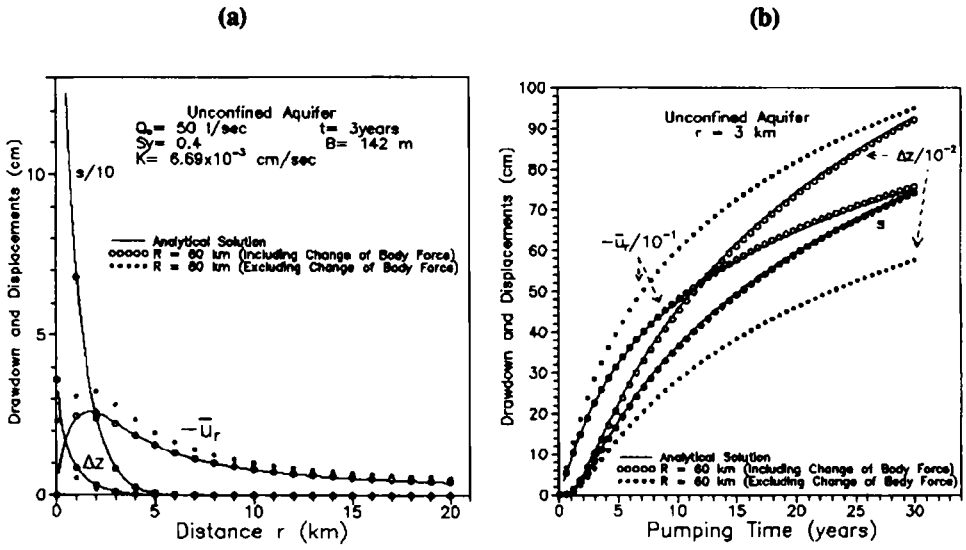

Figure 3. Distribution of the drawdown s, horizontal displacement $\bar{u}_r$ and vertical displacement Δz when pumping from an unconfined aquifer: (a) spatial distribution after continuous pumping for 3 yr and (b) temporal distribution at 3 km from the pumping well

change in body force, all the horizontal displacements are overestimated by 0·136 cm. After continuous pumping for 30 yr, the drawdown, horizontal displacement, and vertical displacement at a distance of 3 km from the well are 74·60, − 7·518, and − 0·929 cm, respectively, when the infinitely horizontal domain is considered. The absolute errors in these estimated values are 0·404, 0·063, and − 0·007 cm, respectively, when $R = 60$ km and including the change in body force. All of the horizontal and vertical displacements shown in Figure 3(b) are overestimated and underestimated by 1.982 and 0.351 cm, respectively, when neglecting the change in body force. It can be observed that the estimated drawdown is nearly unaffected by the change in body force. However, the horizontal and vertical displacements may be, respectively, overestimated and underestimated by neglecting the change in body force. This suggests that the change in body force comes into play once an unconfined aquifer has been pumped, because the displacements occurring in unconfined aquifers are caused not only by the drop of the water table but also by the change in body force.[18] The behaviour of land displacements is similar to that in the confined case when the change in body force is not considered. When the drawdown is small compared to the saturated thickness at any time and when the change in body force is neglected, the displacement quantities are approximately the same for the confined and unconfined aquifers if the values of the storage coefficient and specific yield are assumed to be equal. The storage coefficient is herein defined as the volume of released water per unit pressure decline per unit area surface due to the compaction of aquifer and the expansion of water. Simulation results also show that the drawdown and horizontal displacement at the nodes along the vertical direction are almost the same for both confined and unconfined cases. It coincides with the assumption that the horizontal displacements have no variations along the vertical direction.

Steady state displacements for a point sink pumping from an isotropic/cross-anisotropic porous elastic half-space

A point sink, located at a depth of h below the surface of an aquifer, is assumed to pump at a constant rate Q_w. The formation of the aquifer is assumed to be homogeneous. The initial and boundary conditions for such an aquifer system with $i, j = r, z$ are

$$\begin{aligned}
&t \leqslant 0, \quad r \geqslant 0, \qquad \phi = \phi^0 \quad \text{and} \quad u_r, u_z = 0 \\
&t > 0, \quad r = 0, \qquad u_r = 0 \quad \text{and} \quad \sigma^e_{zj} n_j = 0 \\
&t > 0, \quad r \to \infty, \qquad \phi = \phi^0 \quad \text{and} \quad \sigma^e_{ij} \cdot n_j = 0 \\
&t > 0, \quad z = B, \qquad \phi = \phi^0 \quad \text{and} \quad \sigma^e_{ij} n_j = 0
\end{aligned} \tag{14}$$

The saturated thickness B of the aquifer will approach infinity if the domain of the aquifer is considered to be in a half-space. Tarn and Lu[19] presented analytical solutions for the steady-state displacement and pressure decline due to a point sink pumping from an isotropic/cross-anisotropic porous elastic half-space.

The following data are used to simulate the problem with the present model: $K_z = 6{\cdot}69 \times 10^{-3}$ cm/s; $Q_w = 50$ l/s; $\gamma_w = 9{\cdot}806 \times 10^{-3}$ N/cm^3; $h = 28{\cdot}4$ m; $K_r/K_z = 0{\cdot}5$; $v_{r\theta} = 0{\cdot}0$; $v_{rz} = 0{\cdot}38$; $G_{zr}/E_z = 0{\cdot}38$; $E_r/E_z = 1{\cdot}84$[20]; and $E_z = 1{\cdot}119 \times 10^4$ N/cm^2. The water compressibility β_w is neglected. K_r and K_z are the components for the conductivity tensor in the horizontal and vertical directions, respectively; $v_{r\theta}$ and v_{rz} are, respectively, Poisson's ratios for the horizontal and vertical strains that result from a horizontal stress; E_r and E_z are Young's moduli in the horizontal and vertical directions, respectively; and G_{zr} is the shear modulus in the vertical plane. Young's

modulus E_i characterizes the strain in the i direction produced by stress in the same direction. The shear modulus G_{ij} characterizes the shear strain ε_{ij} produced by the shear stress σ_{ij}. Poisson's ratio v_{ij} characterizes the compressive strain in the j direction produced by a tensile stress in the i direction.

The non-uniform finite element mesh illustrated in Figure 1 is again employed. Near the point sink, both the vertical grid-size Δv and the horizontal grid-size Δr are smaller. At $r = 0$, the sink is located at a depth of h below the surface of the aquifer and the soil is restrained from any lateral movement; however, it is free to move vertically. At the other boundaries, the soil is free to move both horizontally and vertically. The surface of the aquifer is treated as previous so that the Dirichlet boundary for pressure may be specified. The vertical movement at the point P_F in the mesh indicated in Figure 1 is restrained from any vertical movement to avoid generating a singular matrix in numerical simulations.

Results of simulations for the steady-state displacements are shown in Figure 4. Simulations of the chosen normalized boundary depth $B_n = B/h = 1000$ and normalized boundary range $R_n = R/h = 280$, that larger chosen values of B_n and R_n would not change the estimated results, are given in these figures. Analytical solutions[19] for the horizontal displacement and vertical displacement are indicated by the solid lines. At distances of 1 and 2 km from the point sink, the vertical displacements shown in Figure 4 are $-0{\cdot}0217$ and $-0{\cdot}0109$ cm, respectively, when the half-space domain is considered. For $R_n = 280$ and $B_n = 1000$, the absolute errors in estimated vertical displacements at distances of 1 and 2 km are 0·0079 and 0·0078 cm, respectively. The absolute values of relative errors[17] shown in Figure 4 are all less than 17.30% for the horizontal displacements.

Note that trial and error should be used to find reasonable estimates for the displacements when aquifers with half-space are simulated. The normalized boundary range and normalized

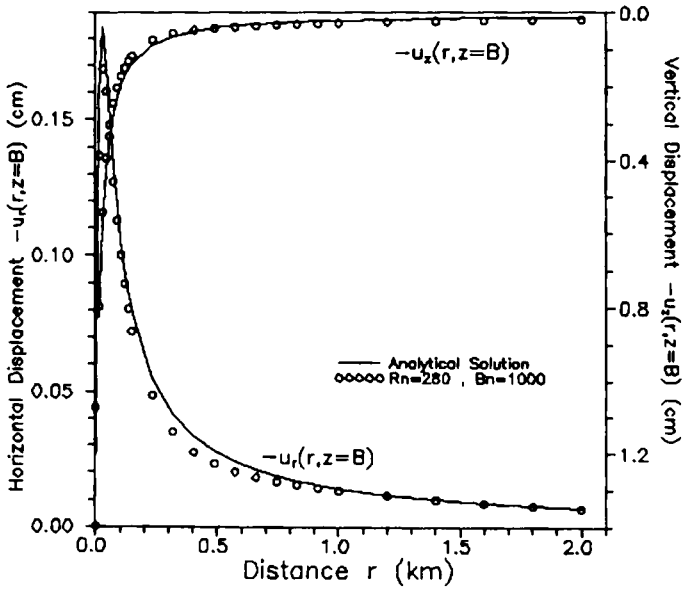

Figure 4. Horizontal distribution for the horizontal and the vertical displacements at the aquifer surface of a cross-anisotropic aquifer

boundary depth should be chosen to where the drawdown in response to the pumping is rather small, so that the simulation results would not change with larger chosen values for those boundary distances.

MODEL PREDICTION ON UNSATURATED MEDIA

The proposed model is capable of dealing with the displacement problems in unsaturated porous media as mentioned previously. The soil displacements due to pressure decline in unsaturated media is predicted in the following case.

Displacements due to pressure decline in unsaturated porous media

A single partially penetrating well of radius r_w is considered to pump at a constant rate Q_w from an unconfined aquifer with horizontal infinite extent. The formation of this aquifer is considered to be homogeneous and isotropic. The initial and boundary conditions for such an aquifer system with $i, j = r, z$ are described as

$$\begin{aligned}
&t \leqslant 0, \quad r \geqslant r_w, \quad \phi = \phi^0 \quad \text{and} \quad u_r, u_z = 0 \\
&t > 0, \quad r \to \infty, \quad \phi = \phi^0 \quad \text{and} \quad \sigma^e_{ij} n_j = 0 \\
&t > 0, \quad z = 0, \quad \frac{\partial \phi}{\partial z} = 0 \quad \text{and} \quad u_z = 0, \quad \sigma^e_{rj} n_j = 0 \\
&t > 0, \quad r = r_w, \quad u_r = 0, \quad \sigma^e_{zj} n_j = 0 \quad \text{and} \quad \frac{\partial \phi}{\partial r} = 0 \quad \text{for } B - H < z < B \\
&\qquad = \frac{Q_w}{2\pi r_w K H} \quad \text{for } 0 < z < H
\end{aligned} \tag{15}$$

where H is the pumping section of the well.

The following data from the paper of Safai and Pinder[6] are used in the simulation: $K = 2{\cdot}0 \times 10^{-4}$ m/s; $\phi^0 = B = 10$ m; $Q_w = 20$ m^3/h; $\gamma_w = \rho g = 9{\cdot}8 \times 10^3$ N/m^3; $n = 0{\cdot}2$; $\nu = 0{\cdot}1$; $G = 10^7$ N/m^2; $\beta_w = 5{\cdot}0 \times 10^{-10}$ N/m^2 and $H = 2{\cdot}5$ m. A non-uniform finite element mesh sketched in Figure 1 is also employed. A uniform vertical grid-size of $\Delta v = 2{\cdot}5$ m is chosen. Horizontal grid-size values Δr are smaller near the well, and gradually increase toward the infinite boundary. At $r = r_w = 0{\cdot}3$ m, a constant flux across the pumping section of the well is specified. The soil is assumed to be restrained from any lateral movement; however, it is free to move vertically at the well boundary. The top boundary is treated as previous and free to move horizontally and verically. The bottom boundary is treated as impervious and is presumed to have no vertical movement; however, the soil is free to move horizontally. At $r = R$, the soil is assumed to be free to move both vertically and horizontally. The unsaturated hydraulic properties of the aquifer will be considered when the pore pressure P becomes negative. The mathematical relationships between the relative hydraulic conductivity K_r, degree of saturation S_w and suction head $\Psi = P/\rho g = \phi - z$ employed in the simulation may be expressed as[6]

$$\begin{aligned}
K_r &= \{1 + (a|\Psi|)^b\}^{-a} \\
S_w &= \frac{\theta_r}{\theta_s} + \left(1 - \frac{\theta_r}{\theta_s}\right)\{1 + (\beta|\Psi|)^\gamma\}^{-\alpha}
\end{aligned} \tag{16}$$

where θ_r is the residual moisture content of soil, θ_s is the saturated moisture content and a, b, α, β and γ are parameters that characterize the properties of soil. The unsaturated hydraulic conductivity may be expressed as $K \cdot K_r$. Those curves of K_r versus $|\Psi|$ and S_w versus $|\Psi|$ shown in Figure 5(a) are utilized for the simulation. Values of those unsaturated soil parameters in equation (16) are $\theta_r = 0{\cdot}031$, $\theta_s = 0{\cdot}2$, $\alpha = 1{\cdot}0$, $\beta = 0{\cdot}017$, $\gamma = 2{\cdot}5$, $a = 0{\cdot}066$ and $b = 5{\cdot}0$.[6] The change in body force is taken into consideration when the moisture content changes in the dewatering zone. The system of equations, which are in terms of P, u_r and u_z,

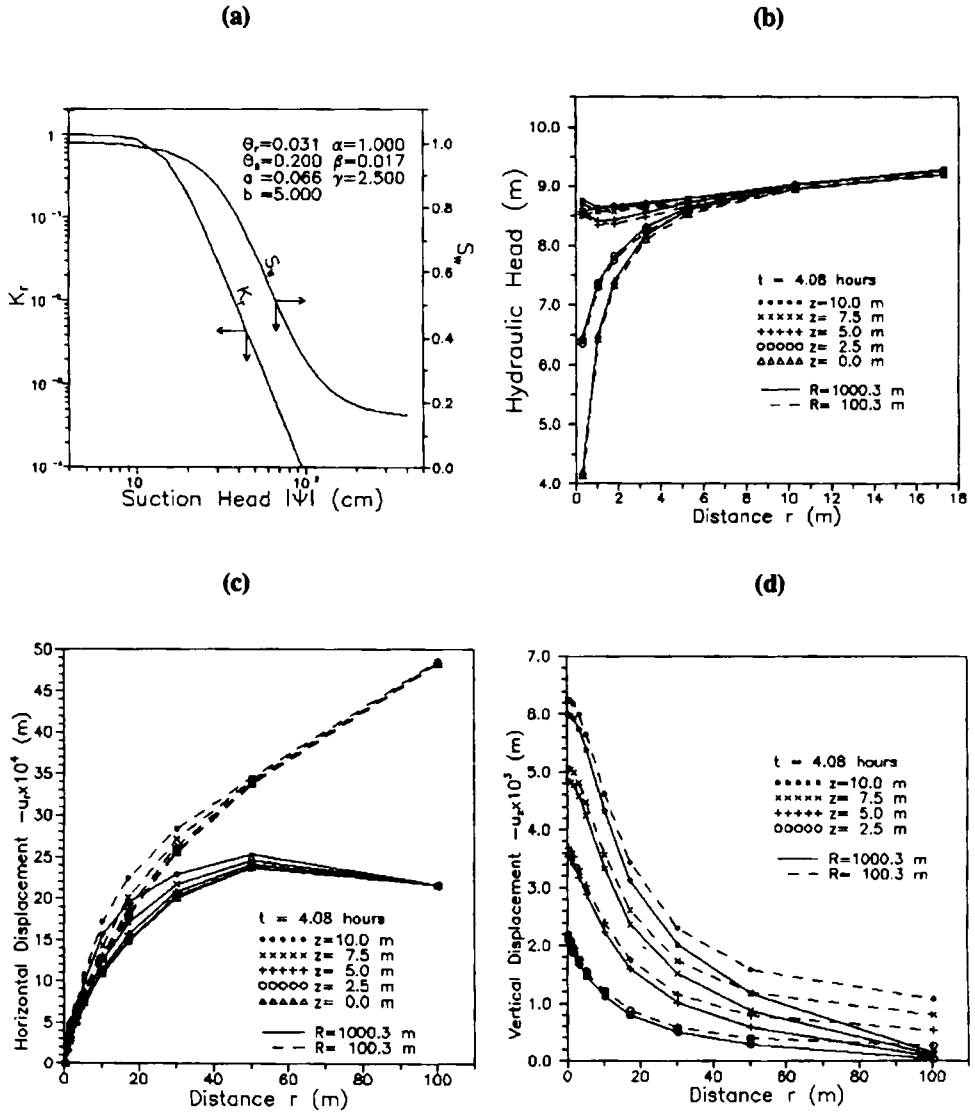

Figure 5. (a) Relationships between the relative hydraulic conductivity K_r, degree of saturation S_w, and suction head $|\psi|$; spatial distribution of (b) the hydraulic head ϕ, (c) horizontal displacement u_r, and (d) vertical displacement u_z after continuous pumping from an unconfined aquifer for 4.08 h

becomes non-linear when aquifers are in an unsaturated condition. The Picard iterative method[21] is utilized to solve this non-linear system. At each time step, the iterations are terminated when all the absolute incremental values of the pressure head and displacements are smaller than 10^{-6} m.

Results of simulations after continuous pumping for 4·08 h are demonstrated in Figure 5. The predicted values of hydraulic head ϕ, horizontal displacement u_r and vertical displacement u_z versus horizontal distance are shown in those figures by indicating the different position in vertical co-ordinate and chosen horizontal boundary range R. The magnitudes of horizontal displacement are found to vary along the vertical positions. The maximum one occurs at the top surface in magnitude of 0·253 cm when R = 1000·3 m is chosen. The maximum magnitude of the vertical displacement is predicted to occur at the top surface of the well in magnitude of 0·600 cm when R = 1000·3 m.

The prediction results are also demonstrated by dashed lines in Figure 5 for R = 100·3 m. Both the horizontal and vertical displacements can be seen here to be significantly overestimated, although the pressure decline deviates slightly from the estimations when choosing R = 1000·3 m. This apparently indicates again that choosing inappropriate horizontal boundary values will affect the estimated values of displacements, as mentioned in the previous studies. It is interesting to note that similar to the phenomena shown in Figure 5(b) when R = 100·3 m, the magnitude of horizontal displacement in Safai and Pinder[6] is found to increase with the distance r from the well. Such a problem is also found in their simulations of pumping from a confined aquifer.[7] Our simulation results indicate that horizontal displacements increase after the start of pumping and tend to decrease beyond a distance of 50 m from the well after continuous pumping for 4·08 h when R = 1000·3 m.

Horizontal boundary range values larger than 1000·3 m were also chosen for simulations. The results, not shown here, were in very close agreement with the one when R = 1000·3 m as shown in Figure 5. It is worth noting that the values chosen for R in the simulations of Safai and Pinder might be not large enough.

BOUNDARY EFFECT PROBLEM

Previous studies in model verification and prediction have shown that the simulation results yielded by the proposed finite element model are apparently affected by the choice of boundary range values for aquifers with infinite domain. Appropriate boundary range values should be chosen based on the maximum duration of simulation, the aquifer properties and the location where the estimation of displacements is required. Methods of boundary elements and infinite elements have been proposed recently to deal with the problems in unbounded domains. Methods coupling finite elements with boundary elements[22] or infinite elements[23, 24] appear to be well suited to modelling physical systems with infinite space. The analysis of boundary elements may be formulated based on the fundamental solutions from the governing differential equation or at least the differential operator. The method of boundary elements has the virtue of reducing the calculation domain and, consequently, needs less computing time and storage requirement. The boundary element approximation was employed by Liggett and Liu[25] to solve flow problems for porous media. The analysis of infinite elements may extend finite elements to infinity by multiplying the basis function of finite elements with decay functions or by mapping a finite domain onto an infinite domain using the mapped infinite elements. This approach retains the same advantages of banded stiffness matrix and numerical integration procedures as the finite element method has. Furthermore, it may be easily implemented into finite element programs and saves substantial computing and time and storage space.[26, 27] It is probably the most economical

means of dealing with the unbounded domain from the standpoint of computation.[28] This approach was utilized by Honjo and Pokharel[26] for seepage analysis and also employed by Simoni and Schrefler[27] to simulate the problems of soil consolidation due to loading.

It is valuable to note that chosen boundary range values may be smaller when using a finite element method coupled with boundary elements or infinite elements. Nevertheless, the analysis of boundary elements may fail to solve the problems for aquifers that are partially saturated and/or heterogeneous in formation because the fundamental solution in the formulation is unavailable. The accuracy of finite element solution may be substantially improved when coupling with infinite elements. However, proper selection of the decay functions or mapping functions requires extensive experience. Those functions should be related to the physical systems of interest and will differ in different cases. Moreover, solution by the infinite element method may not represent the true behaviour in the infinite field where the aquifer properties are heterogeneous.[26] The effects of boundary range selection may still appear after long periods of pumping and simulation.

DISPLACEMENT MECHANISM PROBLEM

All of the previous simulation results indicated that horizontal displacement peaks at some distance from the pumping well and then tends to decrease beyond that distance. This phenomenon may be explained by the analytical solutions for regional cases where a single well pumps from a confined or an unconfined aquifer. A diagram illustrating forces acting on the media in a radial plane is shown in Figure 6. Where σ^e_{rr} and $\sigma^e_{\theta\theta}$ are the incremental total stresses in radial and tangential directions, respectively. The relationship between the stresses and the fluid pressure, equation (3), may be then rewritten by the incremental quantities of superscript $(\cdot)^e$ as $\sigma^e_{ij} = \sigma'^e_{ij} - P^e\delta_{ij}$ with $i, j = r, \theta, z$ in cylindrical co-ordinates. Note that $\sigma^e_{i\theta}$, $\sigma^e_{\theta j}$, $\varepsilon_{i\theta}$, and $\varepsilon_{\theta j}$ may vanish due to axisymmetry when $i, j \neq 0$. The incremental total stresses in two regional cases may

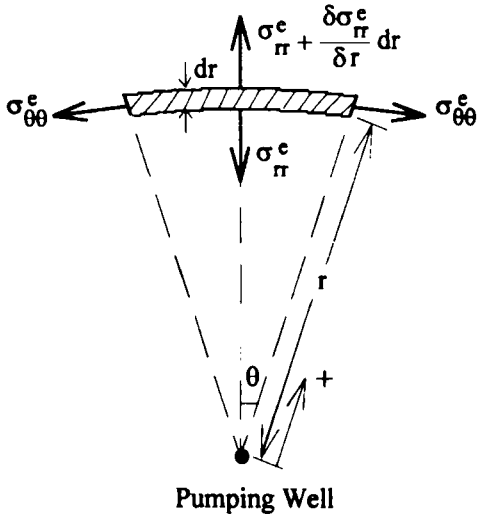

Figure 6. Illustrated diagram for incremental total stresses acting on media in a radial plane

be derived based on the analytical solutions of drawdown and displacements.[18] Those are then obtained in confined aquifers as

$$\sigma^e_{rr} = \sigma'^e_{rr} - P^e = \sigma'^e_{rr} + \rho g s = \frac{\rho g Q_w}{8\pi T}\kappa \mathcal{F}(u) = -2G\frac{u_r}{r} = -2G\varepsilon_{\theta\theta}$$

$$\sigma^e_{\theta\theta} = \sigma'^e_{\theta\theta} - P^e = \sigma'^e_{\theta\theta} + \rho g s = \frac{\rho g Q_w}{8\pi T}\kappa \mathcal{F}'(u) = -2G\frac{\partial u_r}{\partial r} = -2G\varepsilon_{rr} \tag{17a}$$

$$\sigma^e_{zz} = \sigma'^e_{zz} - P^e = \sigma'^e_{zz} + \rho g s = 0$$

and in unconfined aquifers as

$$\sigma^e_{rr} = \sigma'^e_{rr} - P^e = \sigma'^e_{rr} + \rho g s = \frac{\rho g Q_w}{8\pi T}\left(1 - \frac{\lambda S_y}{2G}\right)\kappa \mathcal{F}(u) = -2G\frac{u_r}{r} = -2G\varepsilon_{\theta\theta}$$

$$\sigma^e_{\theta\theta} = \sigma'^e_{\theta\theta} - P^e = \sigma'^e_{\theta\theta} + \rho g s = \frac{\rho g Q_w}{8\pi T}\left(1 - \frac{\lambda S_y}{2G}\right)\kappa \mathcal{F}'(u) = -2G\frac{\partial u_r}{\partial r} = -2G\varepsilon_{rr} \tag{17b}$$

$$\sigma^e_{zz} = \sigma'^e_{zz} - P^e = \sigma'^e_{zz} + \rho g s = -\frac{\rho g S_y Q_w}{4\pi T}W(u) = -\rho g S_y s$$

where σ^e_{zz} is the incremental total stress in the vertical direction; $\sigma'^e_{ii} = 2G\varepsilon_{ii} + \lambda\varepsilon$ with $i = r, \theta, z$; $\varepsilon_{rr} = \partial u_r/\partial r$; $\varepsilon_{\theta\theta} = u_r/r$; $\varepsilon_{zz} = \partial u_z/\partial z$; $\varepsilon = \varepsilon_{rr} + \varepsilon_{\theta\theta} + \varepsilon_{zz}$; $\kappa = G/(\lambda + G)$; $\mathcal{F}(u) = W(u) - e^{-u}/u + 1/u$; $\mathcal{F}'(u) = W(u) + e^{-u}/u - 1/u$; and $W(u)$ is the well function. Equation (17a) with $u = r^2/4C_v t$ and equation (17b) with $u = r^2/4t(S_y/T + 1/C^*_v)^{-1}$ represent the mathematical relations of those incremental total stresses for confined and unconfined cases, respectively, where $C_v = K/\rho g(n\beta_w + 1/(\lambda + G))$ and $C^*_v = K/\rho g(n\beta_w + (1 + S_y/2)/(\lambda + G))$.

By employing the data in previous regional cases, the values of incremental total stresses versus horizontal distance after continuous pumping for 3 yr are shown in Figure 7. Initially, the values

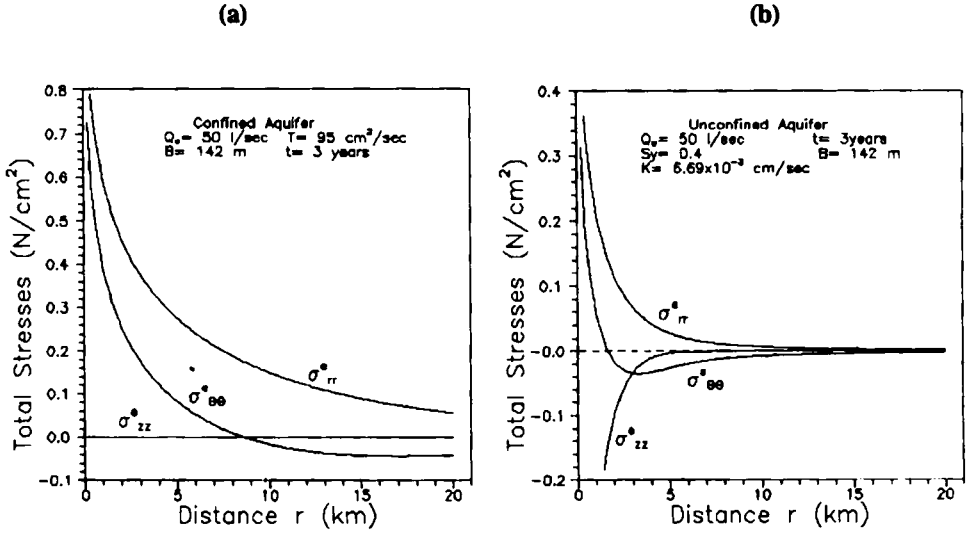

Figure 7. Spatial distribution of incremental total stresses after continuous pumping for 3 yr from (a) a confined aquifer and (b) an unconfined aquifer

of $\sigma^e_{\theta\theta}$ are positive and gradually decrease along the distance r and become negative beyond approximately 8.6 and 1.7 km from the well, respectively, in confined and unconfined cases. Finally, those negative values approach zero when the horizontal distance approaches infinity.

The media as shown in Figure 6 will be forced to move horizontally toward the pumping well as a result of the incremental total stress in the radial direction σ^e_{rr} decreasing with distance r, i.e. $\sigma^e_{rr} + (\delta\sigma^e_{rr}/\delta r)\,dr < \sigma^e_{rr}$ as indicated in Figure 7. It may be seen from equation (17) that the horizontal movement of media toward the pumping well may also be caused by the positive incremental total stress in the tangential direction $\sigma^e_{\theta\theta}$. Note that $\delta\sigma^e_{\theta\theta}/\delta\theta$ vanishes here due to axisymmetry. Contrarily, the horizontal movement of media against the pumping well may occur when the value of $\sigma^e_{\theta\theta}$ becomes negative. Accordingly, the changes of $\sigma^e_{\theta\theta}$ from positive values to negative ones shown in Figure 7 may clarify that the horizontal displacement in regional cases have peak values at distances of approximately 8·6 and 1·7 km from the pumping well, respectively, as indicated in Figures 2 and 3. Similar phenomena for horizontal displacements are indicated in the analytical solution by Tarn and Lu[19] as shown in Figure 4. It is also demonstrated in Figure 5(c) for cases in unsaturated media.

It is intersting to find that the incremental total stress in the vertical direction σ^e_{zz} in equation (17) is equal to zero for the confined case and is equivalent to the change in body force in the dewatering zone for the unconfined case. Apparently, the value of σ^e_{zz} under confined conditions is unchanged when pumping from aquifers and has no influence on the horizontal and vertical displacements. On the other hand, the value of σ^e_{zz} in unconfined aquifers changes with the drop of the water table and affects the horizontal and vertical displacements. This finding indicates that the change in body force in unconfined aquifers should be considered. Otherwise, if the change in body force is neglected, the value of σ^e_{zz} in equation (17b) becomes zero and the second term in the brackets of σ^e_{rr} and $\sigma^e_{\theta\theta}$ in equation (17b), which includes S_y and is introduced by the change in body force, will vanish. The resulting displacement behaviour may be the same as that of a confined aquifer.

CONCLUDING REMARKS

A multidimensional numerical model employing the Galerkin finite element method has been developed to simulate land displacements due to pressure decline in aquifers. The model has been verified by comparing its simulation results with known analytical solutions in three simplified cases. The simulation results of displacements due to pressure decline in unsaturated porous media has also been performed. The ability of the model to simulate the non-linear problems involving land displacement in variably unsaturated media has then been demonstrated with such an example. When problems with infinite domain are simulated, the values of boundary ranges should be chosen based upon the maximum duration of simulation, the aquifer properties, and the location where the estimated displacements is required. Results of numerical simulations indicate that the boundary ranges should be extended to where the drawdown in response to the pumping is rather small if aquifers with infinite domain are pumped. It has also been demonstrated that agreement between numerical and analytical solutions is excellent when the values of the boundary ranges are chosen adequately. The change in body force in the equilibrium equation should be considered once an unconfined aquifer has been pumped. Otherwise, the horizontal and vertical displacements will be, respectively, overestimated and underestimated. Displacements occurring in unconfined aquifers are induced not only by the drop of the water table but also by the change in body force in the dewatering zone. Also, the changes in total stresses were found to be an important factor that affects the land displacement behaviour when pumping aquifers. Simulation results showed a good agreement with the assumption that no variations in

the horizontal displacement would be present along the vertical direction when formulating the regional problem.

ACKNOWLEDGEMENT

This research was supported by the National Science Council of the Republic of China, under grant of NSC 82-0410-E009-198. The authors would like to thank three anonymous reviewers for their valuable and constructive comments.

APPENDIX I

Coefficient matrices in Cartesian co-ordinates

$$C_{11\alpha\beta} = \int N_\alpha \left(n\frac{dS_w}{dP} + nS_w\beta_w \right) N_\beta \, dx\, dy\, dz$$

$$C_{12\alpha\beta} = \int N_\alpha S_w \frac{\partial N_\beta}{\partial x} dx\, dy\, dz$$

$$C_{13\alpha\beta} = \int N_\alpha S_w \frac{\partial N_\beta}{\partial y} dx\, dy\, dz$$

$$C_{14\alpha\beta} = \int N_\alpha S_w \frac{\partial N_\beta}{\partial z} dx\, dy\, dz$$

$$C_{15\alpha\beta} = \int \nabla N_\alpha \cdot \frac{K}{\rho g} \cdot \nabla N_\beta \, dx\, dy\, dz$$

$$C_{21\alpha\beta} = \int -\frac{\partial N_\alpha}{\partial x} S_w N_\beta \, dx\, dy\, dz$$

$$C_{22\alpha\beta} = \int \left[\frac{\partial N_\alpha}{\partial x}(A + 2N)\frac{\partial N_\beta}{\partial x} + \frac{\partial N_\alpha}{\partial y} N \frac{\partial N_\beta}{\partial y} + \frac{\partial N_\alpha}{\partial z} L \frac{\partial N_\beta}{\partial z} \right] dx\, dy\, dz$$

$$C_{23\alpha\beta} = \int \left[\frac{\partial N_\alpha}{\partial x} A \frac{\partial N_\beta}{\partial y} + \frac{\partial N_\alpha}{\partial y} N \frac{\partial N_\beta}{\partial x} \right] dx\, dy\, dz$$

$$C_{24\alpha\beta} = \int \left[\frac{\partial N_\alpha}{\partial x} F \frac{\partial N_\beta}{\partial z} + \frac{\partial N_\alpha}{\partial z} L \frac{\partial N_\beta}{\partial x} \right] dx\, dy\, dz$$

$$C_{31\alpha\beta} = \int -\frac{\partial N_\alpha}{\partial y} S_w N_\beta \, dx\, dy\, dz$$

$$C_{32\alpha\beta} = \int \left[\frac{\partial N_\alpha}{\partial x} N \frac{\partial N_\beta}{\partial y} + \frac{\partial N_\alpha}{\partial y} A \frac{\partial N_\beta}{\partial x} \right] dx\, dy\, dz$$

$$C_{33\alpha\beta} = \int \left[\frac{\partial N_\alpha}{\partial x} N \frac{\partial N_\beta}{\partial x} + \frac{\partial N_\alpha}{\partial y}(A + 2N)\frac{\partial N_\beta}{\partial y} + \frac{\partial N_\alpha}{\partial z} L \frac{\partial N_\beta}{\partial z} \right] dx\, dy\, dz$$

$$C_{34\alpha\beta} = \int \left[\frac{\partial N_\alpha}{\partial y} F \frac{\partial N_\beta}{\partial z} + \frac{\partial N_\alpha}{\partial z} L \frac{\partial N_\beta}{\partial y} \right] dx\, dy\, dz$$

$$C_{41\alpha\beta} = \int -\frac{\partial N_\alpha}{\partial z} S_w N_\beta \, dx\, dy\, dz$$

$$C_{42\alpha\beta} = \int \left[\frac{\partial N_\alpha}{\partial x} L \frac{\partial N_\beta}{\partial z} + \frac{\partial N_\alpha}{\partial z} F \frac{\partial N_\beta}{\partial x}\right] dx\, dy\, dz$$

$$C_{43\alpha\beta} = \int \left[\frac{\partial N_\alpha}{\partial y} L \frac{\partial N_\beta}{\partial z} + \frac{\partial N_\alpha}{\partial z} F \frac{\partial N_\beta}{\partial y}\right] dx\, dy\, dz$$

$$C_{44\alpha\beta} = \int \left[L\left(\frac{\partial N_\alpha}{\partial x}\frac{\partial N_\beta}{\partial x} + \frac{\partial N_\alpha}{\partial y}\frac{\partial N_\beta}{\partial y}\right) + \frac{\partial N_\alpha}{\partial z} C \frac{\partial N_\beta}{\partial z}\right] dx\, dy\, dz$$

$$R_{1\alpha} = \int -\nabla N_\alpha \cdot \mathbf{K} \cdot \nabla z \, dx\, dy\, dz + \int N_\alpha \mathbf{n} \cdot \mathbf{K} \cdot \nabla \phi \, d\Gamma + \int N_\alpha q \, dx\, dy\, dz$$

$$R_{2\alpha} = \int N_\alpha f_x^e \, dx\, dy\, dz + \int N_\alpha [\sigma_{xx}^e n_x + \sigma_{xy}^e n_y + \sigma_{xz}^e n_z] \, d\Gamma$$

$$R_{3\alpha} = \int N_\alpha f_y^e \, dx\, dy\, dz + \int N_\alpha [\sigma_{yx}^e n_x + \sigma_{yy}^e n_y + \sigma_{yz}^e n_z] \, d\Gamma$$

$$R_{4\alpha} = \int N_\alpha f_z^e \, dx\, dy\, dz + \int N_\alpha [\sigma_{zx}^e n_x + \sigma_{zy}^e n_y + \sigma_{zz}^e n_z] \, d\Gamma$$

Coefficient matrices in cylindrical co-ordinates

$$C_{11\alpha\beta} = \int N_\alpha \left(n\frac{dS_w}{dP} + nS_w\beta_w\right) N_\beta r \, dr\, dz$$

$$C_{12\alpha\beta} = \int N_\alpha S_w \left[\frac{\partial N_\beta}{\partial r} r + N_\beta\right] dr\, dz$$

$$C_{13\alpha\beta} = 0$$

$$C_{14\alpha\beta} = \int N_\alpha S_w \frac{\partial N_\beta}{\partial z} r \, dr\, dz$$

$$C_{15\alpha\beta} = \int \nabla N_\alpha \cdot \frac{\mathbf{K}}{\rho g} \cdot \nabla N_\beta \, r \, dr\, dz$$

$$C_{21\alpha\beta} = \int \left[-\frac{\partial N_\alpha}{\partial r} S_w N_\beta r - N_\alpha S_w N_\beta\right] dr\, dz$$

$$C_{22\alpha\beta} = \int \left[\frac{\partial N_\alpha}{\partial r}(A + 2N)\frac{\partial N_\beta}{\partial r} r + \frac{\partial N_\alpha}{\partial r} A N_\beta + N_\alpha A \frac{\partial N_\beta}{\partial r} + (A + 2N)\frac{N_\alpha N_\beta}{r} + \frac{\partial N_\alpha}{\partial z} L \frac{\partial N_\beta}{\partial z} r\right] dr\, dz$$

$$C_{23\alpha\beta} = 0$$

$$C_{24\alpha\beta} = \int \left[\frac{\partial N_\alpha}{\partial r} F \frac{\partial N_\beta}{\partial z} r + \frac{\partial N_\alpha}{\partial z} L \frac{\partial N_\beta}{\partial r} r + N_\alpha F \frac{\partial N_\beta}{\partial z}\right] dr\, dz$$

$$C_{31\alpha\beta} = 0$$

$$C_{32\alpha\beta} = 0$$

$$C_{33\alpha\beta} = 0$$

$$C_{34\alpha\beta} = 0$$

$$C_{41\alpha\beta} = \int -\frac{\partial N_\alpha}{\partial z} S_w N_\beta r \, dr \, dz$$

$$C_{42\alpha\beta} = \int \left[\frac{\partial N_\alpha}{\partial r} L \frac{\partial N_\beta}{\partial z} r + \frac{\partial N_\alpha}{\partial z} F \frac{\partial N_\beta}{\partial r} r + \frac{\partial N_\alpha}{\partial z} F N_\beta \right] dr \, dz$$

$$C_{43\alpha\beta} = 0$$

$$C_{44\alpha\beta} = \int \left[\frac{\partial N_\alpha}{\partial r} L \frac{\partial N_\beta}{\partial r} + \frac{\partial N_\alpha}{\partial z} C \frac{\partial N_\beta}{\partial z} \right] r \, dr \, dz$$

$$R_{1\alpha} = \int -\nabla N_\alpha \cdot \mathbf{K} \cdot \nabla z \, r \, dr \, dz + \int N_\alpha \mathbf{n} \cdot \mathbf{K} \cdot \nabla \phi \, d\Gamma + \int N_\alpha q \, r \, dr \, dz$$

$$R_{2\alpha} = \int N_\alpha f_r^e \, r \, dr \, dz + \int N_\alpha r [\sigma_{rr}^e n_r + \sigma_{rz}^e n_z] \, d\Gamma$$

$$R_{3\alpha} = 0$$

$$R_{4\alpha} = \int N_\alpha f_z^e \, r \, dr \, dz + \int N_\alpha r [\sigma_{zr}^e n_r + \sigma_{zz}^e n_z] \, d\Gamma$$

where x and r co-ordinates are set to be equal.

APPENDIX II

$$[C_{PP}] = \frac{[C_{11}]}{\Delta t} + \theta [C_{15}]$$

$$[C_{Pu_x}] = \frac{[C_{12}]}{\Delta t}$$

$$[C_{Pu_y}] = \frac{[C_{13}]}{\Delta t}$$

$$[C_{Pu_z}] = \frac{[C_{14}]}{\Delta t}$$

$$[C_{u_xP}] = [C_{21}]$$

$$[C_{u_xu_x}] = [C_{22}]$$

$$[C_{u_xu_y}] = [C_{23}]$$

$$[C_{u_xu_z}] = [C_{24}]$$

$$[C_{u_yP}] = [C_{31}]$$

$$[C_{u_yu_x}] = [C_{32}]$$

$$[C_{u_yu_y}] = [C_{33}]$$

$$[C_{u_x u_x}] = [C_{34}]$$

$$[C_{u_x P}] = [C_{41}]$$

$$[C_{u_x u_x}] = [C_{42}]$$

$$[C_{u_x u_y}] = [C_{43}]$$

$$[C_{u_x u_z}] = [C_{44}]$$

$$\{R_P\} = \{R_1\}_t + \left[\frac{[C_{11}]}{\Delta t} - (1-\theta)[C_{15}]\right]\{P\}_{t-\Delta t} + \frac{[C_{12}]}{\Delta t}\{u_x\}_{t-\Delta t} + \frac{[C_{13}]}{\Delta t}\{u_y\}_{t-\Delta t} + \frac{[C_{14}]}{\Delta t}\{u_z\}_{t-\Delta t}$$

$$\{R_{u_x}\} = \{R_2\}_t + [C_{21}]_{t=0}\{P\}_{t=0}$$

$$\{R_{u_y}\} = \{R_3\}_t + [C_{31}]_{t=0}\{P\}_{t=0}$$

$$\{R_{u_z}\} = \{R_4\}_t + [C_{41}]_{t=0}\{P\}_{t=0}$$

where $[\cdot]_{t=0}$ is the coefficient matrix $[\cdot]$ evaluated at the initial time and θ is the time weighting factor. For the Crank–Nicholson scheme, $\theta = 0.5$, and for the backward difference scheme, $\theta = 1$.

REFERENCES

1. A. Verrujit, 'Horizontal displacements in pumped aquifers (abstract)', *EOS Trans. Amer. Geophys. Union*, **51**, 204 (1970).
2. R. W. Lewis, B. A. Schrefler and L. Simoni, 'Coupling versus uncoupling in soil consolidation', *Int. j. numer. anal. methods geomech.*, **15**, 533–548 (1991).
3. M. A. Biot, 'General theory of three-dimensional consolidation', *J. Appl. Phys.*, **12**, 155–164 (1941).
4. J. Bear and M. Y. Corapcioglu, 'Mathematical model for regional land subsidence due to pumping, 2. Integrated aquifer subsidence equations for vertical and horizontal displacements', *Water Resour. Res.*, **17**, 947–958 (1981).
5. M. Y. Corapcioglu and J. Bear, 'A mathematical model for regional land subsidence due to pumping, 3. Integated equations for a phreatic aquifer', *Water Resour. Res.*, **19**, 895–908 (1983).
6. N. M. Safai and G. F. Pinder, 'Vertical and horizontal land deformation in a desaturating porous medium', *Adv. Water Resour.*, **2**, 19–25 (1979).
7. N. M. Safai and G. F. Pinder, 'Vertical and horizontal land deformation due fluid withdrawal', *Int. j. numer. anal. methods geomech.*, **4**, 131–142 (1980).
8. G. Gambolati and R. A. Freeze, 'Mathematical simulation of the subsidence of Venice, 1. Theory', *Water Resour. Res.*, **9**, 721–733 (1973).
9. G. Gambolati, P. Gatto and R. A. Freeze, 'Mathematical simulation of the subsidence of Venice, 2. Theory', *Water Resour. Res.*, **10**, 563–577 (1974).
10. B. A. Schrefler and X. Zhan, 'A fully coupled model for water and airflow in deformable porous media', *Water Resour. Res.*, **29**, 155–167 (1993).
11. A. Lloret, A. Gens, F. Batlle and E. E. Alonso, 'Flow and deformation analysis of partially saturated soils', in E. T. Hanrahan, T. L. L. Orr and T. F. Widdis (eds), *Groundwater Effects in Geotechnical Engineering*, Balkema, Rotterdam, Netherlands, 1987, pp. 565–568.
12. R. W. Lewis and B. A. Schrefler, *The Finite Element Method in the Deformation and Consolidation of Porous Media*, Wiley, New York, 344pp., 1987.
13. J. Bear and M. Y. Corapcioglu, 'Centrifugal filtration in deformable porous media', in *Water Flow in Deformable Porous Media, Report*, Dept. of Civ. Eng., Univ. of Mich., Ann Arbor, 1981.
14. A. Verrujit, 'Elastic storage of aquifers', in R. J. M. DeWiest (ed.), *Flow Through Porous Media*, Academic Press, New York, 1969, pp. 331–376.
15. K. Terzaghi, *Theoretical Soil Mechanics*, Wiley, New York, 510pp., 1943.
16. A. E. H. Love, *A Treatise on the Mathematical Theory of Elasticity*, Dover Press, New York, 1944.
17. C. F. Gerald and P. O. Wheatley, *Applied Numerical Analysis*, 3rd edn. Addison-Wesley, Reading, MO 1984.
18. R. H. Lu and H. D. Yeh, 'Considering the effect of body force for regional land displacements', *Int. j. numer. anal. methods geomech.*, **18**, 145–160 (1994).

19. J. Q. Tarn and C. C. Lu, 'Analysis of subsidence due to a point sink in an anisotropic porous elastic half space', *Int. j. numer. anal. methods geomech.*, **15**, 573–592 (1991).
20. K. M. Lee and R. K. Rowe, 'Deformations caused by surface loading and tunnelling: The role of elastic anisotropy', *Geotechnique*, **39**, 125–140 (1989).
21. P. S. Huyakorn and G. F. Pinder, *Computational Methods in Subsurface Flow*, Academic Press, New York, 1983.
22. O. C. Zienkiewicz, D. W. Kelly and P. Bettess, 'The coupling of the finite element method and boundary solution procedures', *Int. j. numer. methods eng.*, **2**, 355–375 (1977).
23. P. Bettess, 'Infinite elements', *Int. j. numer. methods eng.*, **11**, 53–64 (1977).
24. P. Bettess, *Infinite Elements*, Penshaw Press, Cleadon, 264pp., 1992.
25. J. A. Liggett and P. L.-F. Liu, *The Boundary Integral Equation Method for Porous Media Flow*, George Allen & Unwin Ltd., London, 255pp., 1983.
26. Y. Honjo and G. Pokharel, 'Parametric infinite element for seepage analysis', *Int. j. numer. anal. methods geomech.*, **17**, 45–66 (1993).
27. L. Simoni and B. A. Schrefler, 'Mapped infinite elements in soil consolidation', *Int. j. numer. methods eng.*, **24**, 513–527 (1987).
28. O. C. Zienkiewicz, K. Bando, P. Bettess, C. Emson and T. C. Chiam, 'Mapped infinite element for exterior wave problems', *Int. j. numer. methods eng.*, **21**, 1229–1251 (1985).